



Effect of dispersant on the synthesis of cotton textile waste–based activated carbon by FeCl₂ activation: characterization and adsorption properties

Renzhi Qi¹ · Daofang Zhang¹ · Yuwei Zhou¹ · Yuquan Gao¹ · Mengmeng Xiong¹ · Haixuan Deng¹ · Zhihua Xu¹

Received: 19 May 2020 / Accepted: 29 July 2020 / Published online: 11 August 2020
© Springer-Verlag GmbH Germany, part of Springer Nature 2020

Abstract

Considering the accumulation and high consumption of activating agents, anhydrous ethanol (AE) could be used to dissolve them to improve the dispersion effect, which was an effective way of improving the practical utilization rate. In this study, FeCl₂ was dissolved in AE and further impregnated cotton textile waste (CTW) to prepare activated carbons (ACs) by pyrolysis. Afterward, ACs prepared in optimal conditions determined by the orthogonal experiment evaluated the physicochemical properties and adsorption capacities for Cr(VI). The results illustrated that AE greatly increased the dispersion of FeCl₂ on CTW, reduced the conventional impregnation dosage, and remarkably improved the activation efficiency. Textural analyses revealed that ACs exhibited excellent porosity properties and graphite carbon structure. FeCl₂ catalyzed the decomposition of volatile substances to produce gaseous products and promoted the transformation of amorphous carbon to graphite carbon that was conducive to pore development, followed by the formation of developed micropores and crystal structures. The adsorption performance of ACs was estimated using Cr(VI), and the adsorption was fitted with the pseudo-second-order kinetic and the Langmuir isotherm. Furthermore, the ACs possessed superior magnetization and reusability.

Keywords Cotton textile waste · FeCl₂ · Anhydrous ethanol · Dispersion · Adsorption · Cr(VI)

Responsible Editor: Tito Roberto Cadaval Jr

Highlights

1. The dispersion of anhydrous ethanol reduced the aggregation and dosage of FeCl₂.
2. FeCl₂ dissolved with anhydrous ethanol emerged high activation efficiency.
3. FeCl₂ promoted the formation of microporous and graphite carbon structures.
4. The well-developed activated carbon revealed excellent adsorption and reusability.

Electronic supplementary material The online version of this article (<https://doi.org/10.1007/s11356-020-10321-1>) contains supplementary material, which is available to authorized users.

✉ Zhihua Xu
zhihuaxu_usst@126.com

¹ School of Environment and Architecture, University of Shanghai for Science and Technology, 516 Jungong Rd., Shanghai 200093, People's Republic of China

Introduction

Chromium (Cr) is one of the most toxic heavy metals, primarily existing as Cr(III) and Cr(VI) in the natural environment, and Cr(VI) is more soluble and toxic than Cr(III) (Zhang et al. 2019). Cr(VI) could seriously harm the ecological environment and cause a series of health problems ranging from skin irritation to lung carcinomas (Dong et al. 2017). The threshold of Cr(VI) in the drinking water was limited to 0.05 mg/L as regulated by the World Health Organization (Wu et al. 2013). Therefore, the removal of polluted water with Cr(VI) has become an exigent environmental issue. The conventional physicochemical processes including ion exchange (Han et al. 2020), membrane filtration (Manohara et al. 2019), and adsorption technologies (Monser and Adhoum 2009) were commonly applied to Cr(VI) removal. The removal effect of ion exchange is effective, while its development may be limited by the fact that harmful chemicals may be released into the environment when the resin is regenerated (Muniz et al. 2009). The membrane method exhibits high adaptability, but the cost performance is low because of higher energy requirements (Manohara et al. 2019). Porous carbon or activated

carbons (ACs) are widely used in wastewater purification due to high specific surface area and adsorption performance (Liang et al. 2020). It is worth noting that the differences in the physical structure and chemical composition of the carbon precursor greatly affect the physicochemical properties of ACs (Theydan and Ahmed 2012).

Recently, many researches have been devoted to the preparation of ACs from various precursor materials (Lee et al. 2014; Reguyal et al. 2017). Cotton textile waste (CTW) is rich in cellulose and other substances, which could provide a sufficient carbon source of carbonization. In our previous study, ACs with good surface characteristics were prepared by pyrolysis with chemical activation of CTW (Tian et al. 2019; Xu et al. 2018). To further improve the structural characteristics and surface properties of ACs, chemical activation is considered a highly efficient method. At present, acid, alkali, and metal ions have been used as activating agents to prepare well-developed ACs (Wang and Wang 2019). Nevertheless, it is difficult to recover or separate materials after using ACs as adsorbent (Reguyal et al. 2017). In recent years, the development of magnetic ACs has aroused great interest. It can be recycled by the magnetic field after adsorption and removal of special pollutants (Devi and Saroha 2014). It has been found that magnetic ACs can be prepared by impregnation of precursor materials with HCl aqueous solutions of either FeCl_3 or FeCl_2 at various concentrations and pH values (Muniz et al. 2009). FeCl_3 has been widely used to synthesize magnetic ACs, and the activation mechanism is relatively mature (Xu et al. 2019). So far, some researches have studied FeCl_2 and found that Fe^{2+} could catalyze the production of a large amount of small-molecule gas products, thereby bringing more excellent pore structure to ACs (Wang et al. 2007). Moreover, compared with FeCl_3 , FeCl_2 exhibits better impregnation on raw materials (Ohmukai et al. 2008). Thus, FeCl_2 might have a more efficient activation capacity, and its activation effect should be further studied. However, there is a great concern about the accumulation of activating agents in the activation process, as well as about the high proportion of its in one-step activation pyrolysis, which caused relatively inferior utilization rate and corrosion of pyrolysis equipment. Specifically, since water is used as the solvent, additional hydrogen bonds in water may affect the surface area of FeCl_2 , resulting in high particle agglomeration (Raiteri et al. 2004). It could be found that it is feasible to maintain homogeneous and stable dispersions of FeCl_2 in the impregnation process. Therefore, the dispersity of FeCl_2 should be improved in this process.

Dispersity issues can be eradicated using suitable dispersants by an economical and feasible way to achieve their effective utilization (Tseng et al. 2011). At present, several types of dispersants have been used for dispersing particles and improving their properties (Li et al. 2018b). The dispersant was only used in the impregnation process, mainly to alleviate

the accumulation of FeCl_2 . Besides, it is important to pay attention to the properties of dispersants to prevent the introduction of impurities to affect the subsequent AC adsorption application. Hence, traditional alcohol dispersant is suitable, and its cheap properties could also control the cost. Most important, excellent volatilization of ethanol at low temperatures had little influence on subsequent FeCl_2 activation of CTW (Feng et al. 2020). Furthermore, previous reports showed that the stability of pure ethanol dispersion was higher than that of other dispersion under the different proportions of ethanol and water (Ilyas et al. 2014). Thus, given the influence of hydrogen bond in water, anhydrous ethanol (AE) was used to disperse FeCl_2 .

In this work, FeCl_2 is an activating agent to synthesize ACs from cotton textile waste. Considering the aggregation of FeCl_2 on CTW, AE dispersant was used to replace deionized water to improve its activation effect. An orthogonal experimental method was applied to optimize the mass ratio of FeCl_2 to CTW, the activation temperature, and the activation time for the preparation of ACs. In more detail, the objectives of this paper were (i) to evaluate the effect of AE dispersion on the activation efficiency of FeCl_2 and (ii) to assess the adsorption performance of ACs for Cr(VI) by adsorption kinetics, isotherm.

Materials and methods

Materials

Cotton textile waste (CTW) was obtained from Shanghai Shuangou Textile Co., Ltd. (China). Analytical-grade $\text{K}_2\text{Cr}_2\text{O}_7$, $\text{C}_2\text{H}_6\text{O}$, $\text{FeCl}_2 \cdot 4\text{H}_2\text{O}$, HCl, HNO_3 , H_2SO_4 , and NaOH were purchased from Sinopharm Chemical Reagent Co., Ltd.

Preparation

The synthesis procedure of activated carbons was as follows: the CTW was cut into pieces with an average size of 5 mm, and 2.5 g of pretreated CTW was fully immersed in the determined FeCl_2 solution dissolved in 25 mL of anhydrous ethanol or deionized water (a mass ratio of FeCl_2 : CTW from 0.5:1 to 1.5:1) and sealed the solution at 20 °C for overnight. Then, the mixture was placed in a vacuum oven at 60 °C for 12 h. Afterwards, the mixture was heated in a tube furnace with N_2 atmosphere at a flow rate of 100 mL/min from room temperature to the designated temperature (600–800 °C) at 10 °C/min and maintained for different activation time (1–3 h). The obtained sample was immersed in boiling HCl solution (1.0 mol/L) for 10 min and then washed with deionized water until the pH value of the effluent was close to neutral. Finally, after drying for 12 h in an oven at 105 °C, all as-

prepared carbons were prepared and stored in a vacuum for reserve. Samples synthesized by dissolving with AE were marked as *x-y-z* (*x* is the mass ratio of FeCl₂/CTW, *y* is the activation temperature, and *z* is the activation time). AC prepared in optimal conditions based on orthogonal experimental (mass ratio 0.5:1, activation temperature 600 °C, and activation time 1 h) was named as AC-AE. The sample for dissolving FeCl₂ in deionized water under the same optimal conditions was called AC-DI. Besides, FeCl₂ was used to impregnate CTW, but the dissolution method of FeCl₂ was different. As FeCl₂ was dissolved in deionized water, it is considered as impregnation scheme D, while the dissolution after AE was determined as the impregnation scheme E.

Characterization

The iodine number determination of the ACs was measured according to the Chinese National Standards (GB/T 12496.8–1999). The morphological properties of the CTW and ACs were detected using a scanning electron microscope (HITACHI/S4800, Japan). The pore development of the ACs was explored using N₂ adsorption/desorption isotherms at 77 K, employing a surface area analyzer (Quantachrome/autosorb-iQ-2MP, USA). The total pore volume (*V*_{total}) was determined as the adsorption volume at 0.99 *P*/*P*₀. The micropore surface area (*S*_{micro}) and micropore volume (*V*_{micro}) were calculated using the *t*-method. The pyrolysis behavior of CTW, CTW, and FeCl₂ (H₂O/C₂H₆O) mixtures was carried out by thermogravimetric (TG) analyzer (TGA-1250, USA) in N₂ atmosphere (100 mL/min), heated at the rate of 10 °C/min to reach 600 °C, and kept the temperature for 1 h. The crystal structures of the ACs were measured using an X-ray diffractometer (Bruker/D8 ADVANCE, Germany) at 40 mA and 40 kV with Cu Kα radiation and recorded from 5 to 80° (2θ) at a scanning rate of 3°/min. The surface chemistry of the ACs was determined using a Fourier transform infrared spectrometer (FTIR Bruker/Tensor 27, Germany) over the spectral range from 400 to 4000 cm⁻¹. The point of zero charges (pH_{pzc}) of the ACs was measured by the mass titration (Islam et al. 2017a), where 1 g of ACs was added to 10 mL of deionized water for 24 h, and the pH of the mixture was the value of pH_{pzc}. Magnetic measurements were determined with a vibrating sample magnetometer (VSM, quantum) at 300 K. The field-dependent magnetization curves were calculated between ± 20 kOe. The yield was defined as the ratio of the mass of ACs to that of CTW, which could be explained by Eq. (1):

$$\text{Yield}(\%) = \frac{W_c}{W} \times 100\% \tag{1}$$

where *W* is the weight of CTW; *W*_{*c*} is the weight of the final AC sample after washing and drying.

Orthogonal experiment

The orthogonal experimental design was carried out to obtain the optimal experimental conditions of the ACs. The arranged mixed-level table is shown in Table 1. Letters of A, B, and C were denoted to mass ratio, activation temperature, and activation time, respectively. It should be noted that FeCl₂ used in this experiment was all impregnated by AE.

Adsorption experiments

Effects of pH

The initial pH values of Cr(VI) solutions were adjusted with the range pH 2–7 by NaOH (0.1 mol/L) and HNO₃ (0.1 mol/L). Then, 0.1 g ACs was added to the Cr(VI) solution (50 mg/L, 50 mL), and the reaction was conducted at 25 °C and 150 rpm in a shaker. After 12 h, the solution was taken out and filtered with a 0.45-μm filter membrane, and then its absorbance was measured by a spectrophotometer (UV-Vis, Shanghai Jingke Scientific Instrument Co., Ltd., UV-754, China) according to the Chinese National Standard (GB/T7467-87). The adsorption capacity (*q*) and removal rate (*R*) of Cr(VI) by ACs were calculated by Eqs. (2) and (3):

$$q = \frac{(C_0 - C_t) \times V}{m} \tag{2}$$

$$R = \frac{(C_0 - C_t)}{C_0} \times 100\% \tag{3}$$

where *C*₀ (mg/L) and *C*_{*t*} (*I* = *e*) (mg/L) are the initial and equilibrium concentrations of Cr(VI), respectively; *V* (L) is the volume of the solution, and *m* (g) is the dry weight of ACs.

Adsorption kinetics

Adsorption kinetic experiments were carried out by adding 0.1 g of ACs to 50 mL of solution (50 mg/L) with pH = 2, and the adsorption processes were carried out in a shaker at 25 °C and 150 rpm, but with different contact time (10, 30, 60, 120, 240, 360, or 720 min). Then, the concentration of Cr(VI)

Table 1 Factors and levels of the orthogonal experiment

Levels	Factors		
	A Mass ratio (FeCl ₂ :CTW)	B Activation temperature (°C)	C Activation time (h)
1	0.5	600	1
2	1	700	2
3	1.5	800	3

was measured, and the specific operation could be referred to “Effects of pH.” The adsorption capacity of different contact times was calculated by Eq. (2), where C_t ($I = t$) is the concentration at that time t (h). To study the adsorption kinetic characteristics of ACs on Cr(VI), two kinetic models were proposed to fit the kinetic experimental data, which could be expressed in Eqs. (4) and (5):

$$\text{Pseudo-first-order model : } \ln(q_e - q_t) = \ln q_e - k_1 t \quad (4)$$

$$\text{Pseudo-second-order model : } \frac{t}{q_t} = \frac{1}{k_2 q_e^2} + \frac{t}{q_e} \quad (5)$$

where q_e and q_t (mg/g) are the adsorptive capabilities at equilibrium and time t , respectively, and k_1 (min^{-1}) and k_2 ($\text{g}/(\text{mg min})$) are the rate constants of the pseudo-first- and second-order models, respectively.

Adsorption isotherms

Adsorption isotherm experiments were conducted by adding 0.1 g of ACs to 50 mL of different initial concentrations of solution (50, 100, 200, 400, or 600 mg/L) with pH=2; the reaction was conducted at 25 °C and 150 rpm in a shaker. After adsorption, the concentration of Cr(VI) was measured, whose operations were detailed in the “Effects of pH.” The equilibrium concentration was calculated by Eq. (2). To analyze the Cr(VI) adsorption behavior of ACs, two adsorption isotherm models were proposed to fit the experimental data, which could be expressed in Eqs. (6) and (7):

$$\text{Langmuir model : } q_e = \frac{q_m K_L C_e}{1 + K_L C_e} \quad (6)$$

$$\text{Freundlich model : } q_e = K_F C_e^{\frac{1}{n}} \quad (7)$$

where C_e (mg/g) is the equilibrium Cr(VI) concentration, q_e (mg/g) is the adsorptive capabilities at the equilibrium of Cr(VI), q_m (mg/g) is the maximum adsorptive capability, K_L (L/mg) is the Langmuir affinity constant, and n and K_F ($(\text{mg}/\text{g}) (\text{mg}/\text{L})^{-1/n}$) are the Freundlich constants corresponding to the adsorption intensity and capability, respectively.

Reusability

The synthesis of magnetic activated carbon (MAC) was basically consistent with the procedure of AC-AE; the main difference was that MAC was washed repeatedly by deionized water instead of pickling. For adsorption of MAC, the similar procedures were performed, but the difference was the amount of adsorbent and adsorbate used (0.4 g, 200 mL); the details were described in “Effects of pH.” To evaluate the reusability and stability of MAC, the cycle number-dependent adsorption capacities were checked for 50 mg/L of Cr(VI) (200 mL). The details were as follows: the saturated MAC with Cr(VI)

was dispersed in 50 mL of eluent (0.2 mol/L NaOH) at 25 °C and 150 rpm in a shaker for 12 h. Afterward, the solid materials were collected by an external magnetic field, thoroughly washed with deionized water, then soaked it in H_2SO_4 solution (50 mL, pH=3) for 2 h for activation and reused in the next run of adsorption.

Results and discussion

Orthogonal experimental analysis

The mixed-level orthogonal table L9 (3^4) was presented. The mixed-level orthogonal array was an experimental design method dealing with multi-factors and multi-levels. The analysis of range was calculated by the difference between the maximum and minimum of the averages for each factor.

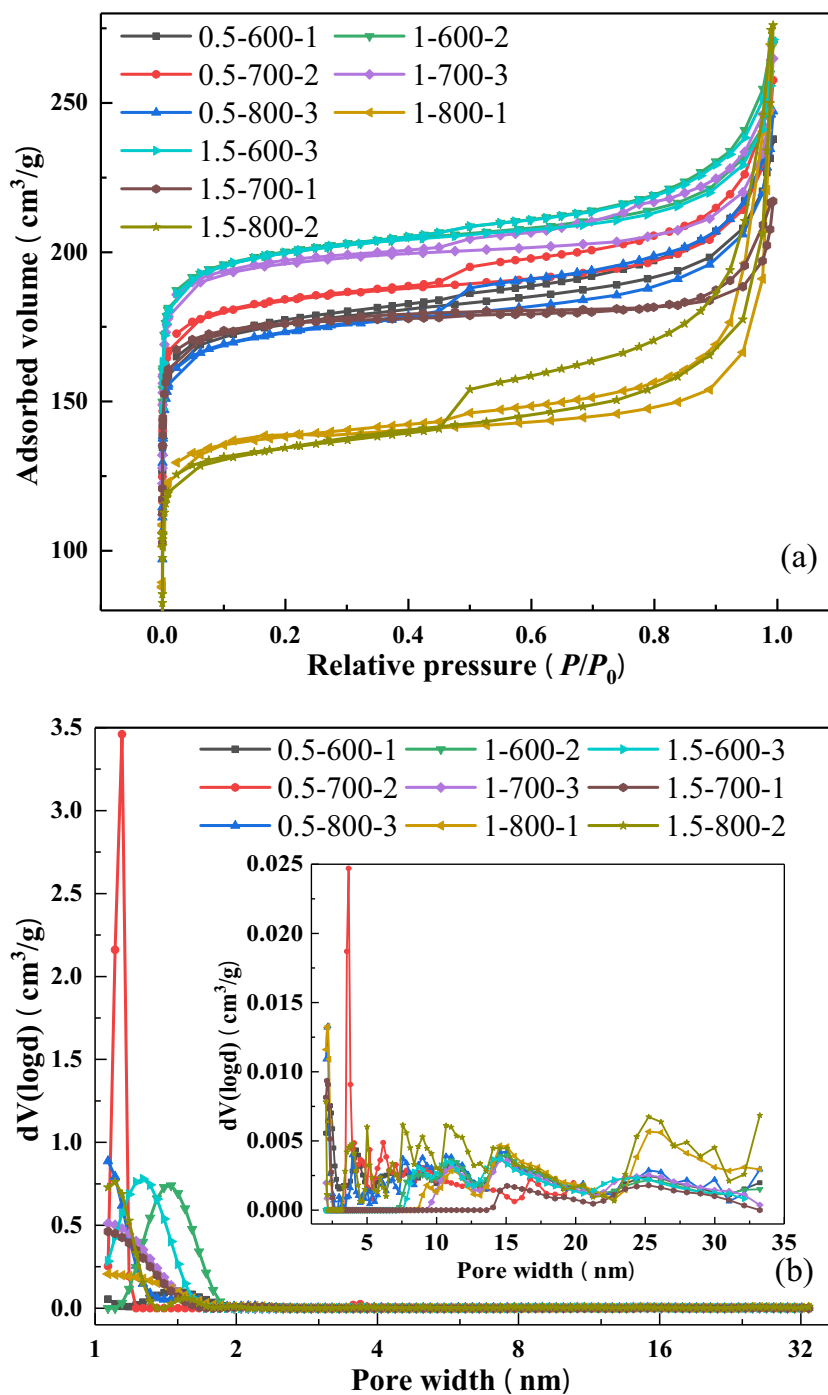
Specific surface area

The results of mixed-level orthogonal arrays design are displayed in Table 2. The specific surface areas (response value) of ACs were measured, which were between 526.361 and 789.540 m^2/g . The N_2 adsorption/desorption isotherm of samples is shown in Fig. 1a. It could be found that the ACs have displayed type I isotherm (when $P/P_0 < 0.4$) and H_4 hysteresis loops (when $P/P_0 > 0.4$) by the IUPAC classification, indicating the presence of prominent microspores and slight amounts of mesoporous (Lam et al. 2017; Lee et al. 2014). With the rise of mass ratio or activation temperature (e.g., 1.5-800-2 and 1-800-1), the relative pressure ranges corresponding to the hysteresis loop became wider, which suggested the occurrence of pore widening in ACs along with the formation of mesopores (He et al. 2012). Overall, the ACs had more developed microporous structures, while the mesoporous

Table 2 The results of mixed-level orthogonal array design for pyrolysis pretreated ACs

Run	Factors			Response
	A	B (°C)	C (h)	Surface area (m^2/g)
1	0.5	600	1	691.579
2	0.5	700	2	726.622
3	0.5	800	3	681.929
4	1	600	2	789.015
5	1	700	3	778.555
6	1	800	1	541.721
7	1.5	600	3	789.540
8	1.5	700	1	698.376
9	1.5	800	2	526.361

Fig. 1 N₂ adsorption/desorption isotherms (a) and pore size distributions (b) of ACs



were slight, which was coherent to the pore size distributions in Fig. 1b. Meanwhile, Table 2 presents that 1.5-800-2 and 1-800-1 exhibited relatively lower specific surface areas of 526.361 m²/g and 541.721 m²/g due to the destruction of the produced microspore walls (Siddiqui et al. 2018). In impregnation scheme E, dissolved FeCl₂ might exhibit superior accessibility to CTW, and its reasonable distribution could ensure that CTW could be carbonized completely and stably to

produce ACs, whereas severe activation conditions might be detrimental to the development of AC pore structure. Notably, 0.5-700-2 showed an abundant microporous structure in the range of 1.0–1.3 nm, which was accompanied by mild reaction conditions. The high-efficiency dispersion of AE alleviated the agglomeration effect of FeCl₂, improved its activation effect, and correspondingly affected the reaction conditions, which was analyzed in detail below (Tseng et al. 2011).

Analysis of range

To determine the optimization of preparation conditions, it was proposed to use the range analysis method to process the ACs and synchronously analyze the influence of three factors on AC performance in Table 3 and Fig. 2 (Xia et al. 2019). Range analysis results showed that the influence of factors on the overall point in decreasing order was activation temperature (B) > activation time (C) > mass ratio (A). Notably, the least influential factor was the mass ratio. In this study, FeCl₂ in the liquid phase was actively absorbed by AE and was uniformly attached on the surface of CTW, which could make full contact with CTW and improve the subsequent activation effect (Shi et al. 2019). Meanwhile, the natural thermodynamic instability of AE led to the enhancement of electrostatic repulsion and steric hindrance, which reduced the potential FeCl₂ accumulation (Tseng et al. 2011).

Figure 2 displays the effect of the three factors on the specific surface area according to the range results. It can be seen that lower FeCl₂ dosage could achieve better specific surface area, mainly because the use of AE reduced the conventional dosage of activating agent. However, as the mass ratio further increased, the specific surface area of ACs decreased. An explanation for this might be that a high dosage of FeCl₂ caused excessive activation (Liew et al. 2018). The pore structure formed in ACs was destroyed, and AE might aggravate this effect. Therefore, the dosage of FeCl₂ and the effect of AE should be considered comprehensively. With the activation temperature increasing, the specific surface area of ACs sharply decreased. This directly confirmed the positive effect of AE on the preparation of ACs in the pyrolysis process. Generally, the higher temperature was required to completely carbonize the precursor due to the uneven distribution and partial aggregation of the activating agent (Wang and Wang 2019). Because FeCl₂ was fully dispersed on CTW, the optimal

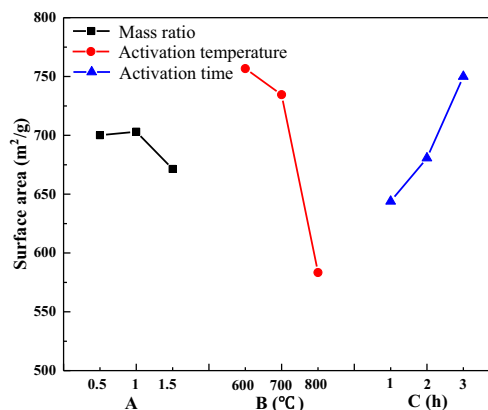


Fig. 2 The effects of different preparation conditions on the surface area

condition could be reached stably and smoothly. With the further increase of activation temperature, the specific surface area decreased dramatically. During pyrolysis, FeCl₂·4H₂O could undergo dehydration, dechlorination, and iron species evolution and transform into Fe₂O₃ and Fe₃O₄ (Ohmukai et al. 2008). Additionally, the iron oxides could consume the carbon matrix, destroying the pore structure in ACs (Rufford et al. 2010). In this way, the requirement of activation temperature for the preparation of ACs was slight with the effect of AE. As the extension of activation time, the specific surface area increased appreciably. It could be objectively observed from Fig. 1b that the prepared ACs under the condition of long activation time emerged more mesopores, which were not conducive to the subsequent adsorption application of ACs (Lee et al. 2014). As discussed above, the use of impregnation scheme E might help CTW to adequately carbonize earlier. Consequently, long activation time might not be beneficial to the development of AC pore structure.

Based on this study, it can be seen that the mass ratio had the lowest effect, and the lowest mass ratio could be used to further control the dosage of the activator. FeCl₂ was more suitable at a lower temperature, which was fully satisfied at 600 °C. To prepare ACs with better microporous properties and avoid excessive energy consumption as much as possible, shorter activation time was enough. Therefore, the optimal factorial combination concluded the activation temperature of 600 °C, the mass ratio of 0.5:1, and the activation time of 1 h. Next, the AC-AE and AC-DI prepared under optimal conditions were characterized and analyzed.

Characteristics

Pyrolysis behavior

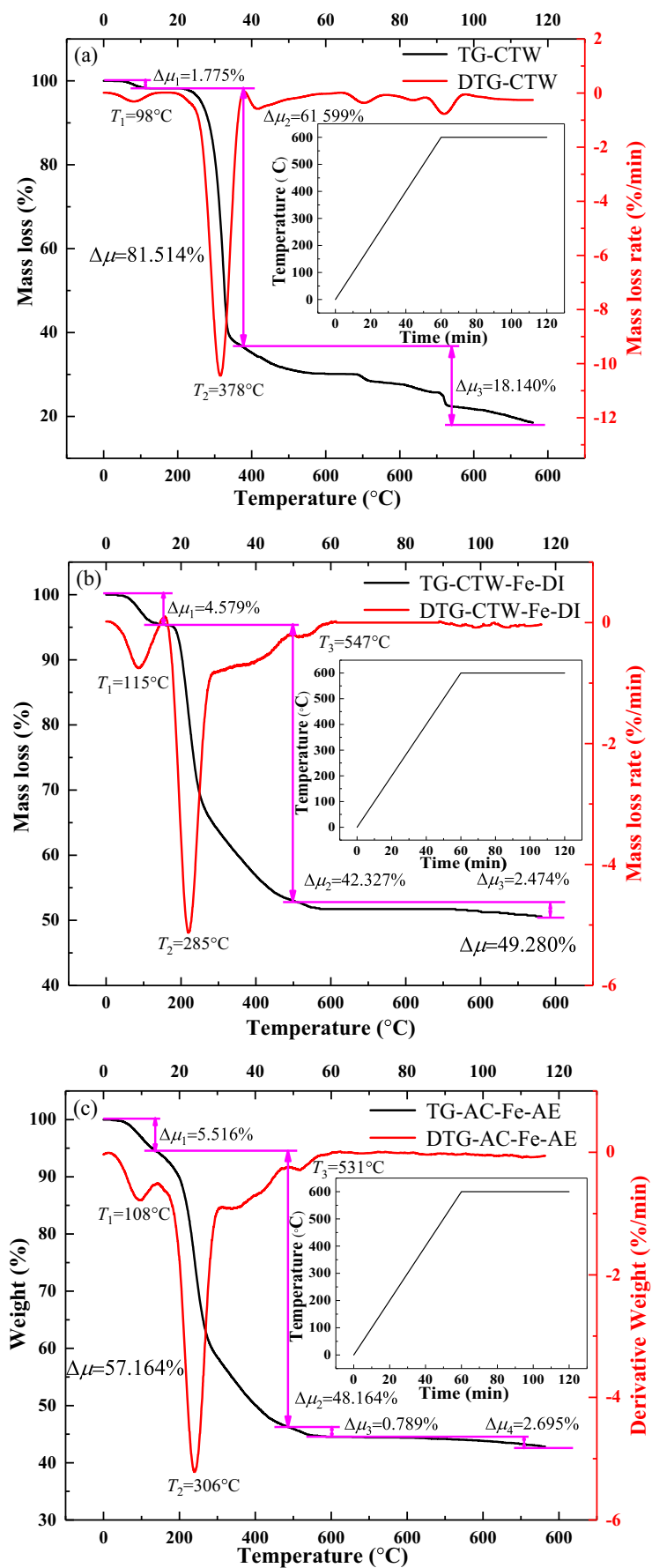
To simulate the preparation process of ACs, the TG-DTG curves of CTW and FeCl₂-impregnated samples (CTW-Fe-AE and CTW-Fe-DI) are presented in Fig. 3, and the influence of different impregnation schemes on pyrolysis was further

Table 3 The range analysis of the overall evaluation point of ACs

Sources	Factor		
	A	B	C
M_1	$M_{11} = 2100.130$	$M_{12} = 2270.134$	$M_{13} = 1931.676$
M_2	$M_{21} = 2109.291$	$M_{22} = 2203.553$	$M_{23} = 2041.998$
M_3	$M_{31} = 2014.277$	$M_{32} = 1750.011$	$M_{33} = 2250.024$
m_1	$m_{11} = 700.043$	$m_{12} = 756.711$	$m_{13} = 643.892$
m_2	$m_{21} = 703.097$	$m_{22} = 734.518$	$m_{23} = 680.666$
m_3	$m_{31} = 671.426$	$m_{32} = 583.337$	$m_{33} = 750.008$
R_j	31.671	173.374	106.116

M_{ij} ($i, j = 1, 2, 3$) was the sum of the data of level i under column j . m_{ij} ($i, j = 1, 2, 3$) was the average value of m_{ij} . Range R_j was the difference between the maximum value and the minimum value of the average value of the corresponding experimental value in column j

Fig. 3 TG and DTG curves of CTW (a), AC-Fe-DI (b), and AC-Fe-AE (c)



studied. In Fig. 3a, the thermal degradation of CTW could be divided into three sections. The first mass loss at about 98 °C was mainly caused by the evaporation of moisture. The second stage from 120 to 390 °C observed the major mass loss of 61.599% which might be due to the decomposition of relatively easily decomposable compounds in CTW such as hemicellulose, cellulose, protein, carbohydrate, and partial decomposition of lignin (Yang et al. 2019). The final stage (390–600 °C) of CTW was probably caused by the continuing carbonization of CTW.

In Fig. 3b, CTW-Fe-DI presented different pyrolysis behavior compared with CTW. The initial DTG peak at about 115 °C and mass loss (4.279%) were both higher than that of CTW (98 °C, 1.775%), because of the evaporation of the crystallization water in $\text{FeCl}_2 \cdot 4\text{H}_2\text{O}$. In the second stage (150–450 °C), CTW-Fe-DI displayed a mass loss (42.327%), and the strong DTG peak at around 285 °C was obviously lower than that of CTW (378 °C). With the activation of FeCl_2 , the volatile components in CTW rapidly underwent decomposition and subsequent polymerization, in which small molecular gases (CO_2 , CO , H_2O) and aromatic substances were produced, thereby reducing the pyrolysis temperature and mass loss in this stage (Cagnon et al. 2009). In fact, these aromatic substances were further decomposed at higher temperatures (400–500 °C) due to the presence of benzene rings, which could also be seen from the DTG that the second stage of CTW-Fe-DI crossed a wider temperature range (150–450 °C) (Cagnon et al. 2009). The third stage (450–600 °C) mass loss (2.474%) of CTW-Fe-DI was lower than that of CTW (18.140%). The presence of iron species might catalyze the formation of iron oxides (Fe_2O_3 , Fe_3O_4) under the pyrolysis condition, consume carbon matrix, and subsequently form a stable iron-carbon matrix structure; thus, this stage showed less mass loss (Rufford et al. 2010).

As seen in Fig. 3c, under impregnation scheme E, the pyrolysis of CTW-Fe-AE could be divided into three stages, while there were many differences with CTW-Fe-DI. The first mass loss (5.516%) was higher than that of CTW-Fe-DI, and the temperature corresponding to the peak also decreased (108 °C) because the aggregation effect of FeCl_2 was weakened, and more crystallization water was released. It could be found that the second stage of degradation begun rapidly after the evaporation of moistures. It was indicated that FeCl_2 and CTW were fully contacted in the dissolution of AE, which could rapidly catalyze the degradation of CTW (Cagnon et al. 2009). Moreover, the mass loss of this stage (48.164%) was higher than that of CTW-Fe-DI (42.327%), which was attributed to the dispersion effect of AE. In the pyrolysis process, the uniformly distributed FeCl_2 promoted the dehydration and polymerization of CTW, which adequately decomposed volatile substances. Besides, more FeCl_2 was involved in the evolution of iron species, resulting in the peak for temperature lasting to 308 °C (Ohmukai et al. 2008). The

final mass loss of CTW-Fe-AE was 3.484%, higher than that of CTW-Fe-DI (2.474%), and the residual mass also decreased (42.836% vs. 50.720%). FeCl_2 dissolved in AE improved CTW to obtain sufficient pyrolysis and carbonization, showing more mass loss in this stage, which indirectly revealed the advantages of solving the aggregation effect of FeCl_2 . Overall, it was confirmed the high efficiency of FeCl_2 in impregnation scheme E.

Pore development

Figure 4 reveals the N_2 adsorption/desorption isotherms of the ACs. The pore structure characteristics are presented in Table 4. It can be found that both ACs showed microporous structure by the type I isotherms of IUPAC classification, and AC-AE showed more abundant micropores, while AC-DI showed more obvious H_4 hysteresis, revealing more mesopores (Islam et al. 2017b). It has been reported that FeCl_2 particularly catalyzed the formation of small-molecule gaseous, which were beneficial to the formation of the pore structures of the carbon matrix (Yang et al. 2019). The dissolution of AE could promote the effect of FeCl_2 , which created a more microporous structure of AC-AE. The AC-AE contained a higher surface area (691.579 m^2/g) and a micropore area (637.106 m^2/g). Moreover, Table 4 shows that AC-DI had higher total pore volume (V_{tot}) and average pore diameter (D_p) than AC-AE and lower microporosity ($S_{\text{mic}}/S_{\text{BET}}$) because of the expansion of partial micropores in AC-DI into mesopores (An et al. 2018). It could be seen that the dissolution of AE effectively reduced the effect of pore expansion caused by FeCl_2 accumulation. Hence, the microporous ACs could be prepared by impregnation scheme E, which might provide more adsorption sites.

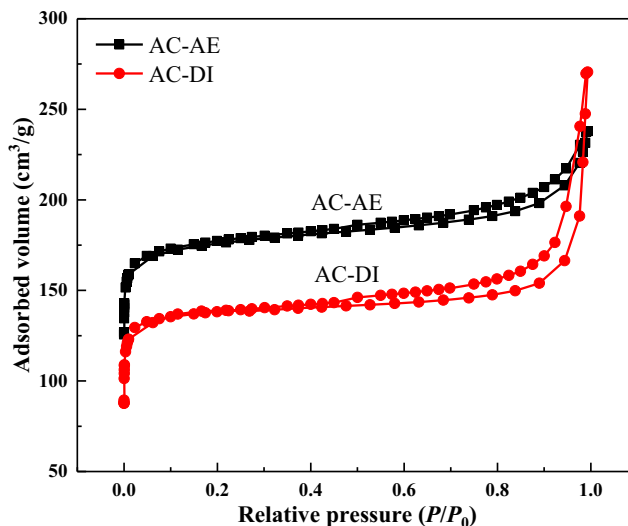


Fig. 4 N_2 adsorption/desorption isotherms of ACs

Table 4 Surface area and pore volume of ACs

Samples	S_{BET} (m ² /g)	S_{mic} (m ² /g)	$S_{\text{mic}}/S_{\text{BET}}$ (%)	V_{tot} (cm ³ /g)	D_p (nm)
AC-AE	691.579	637.106	92.123	0.368	2.128
AC-DI	541.721	523.882	96.707	0.419	3.091

Morphology

Figure 5 provides the SEM micrographs of AC-AE and AC-DI. As shown in Fig. 5a, the AC-AE exhibited heterogeneous surface morphology with a porous structure, indicating the high activation efficiency of FeCl₂. In Fig. 5b, the external surface of AC-DI was smooth and low porosity, although cracks on the surface were more prominent. In impregnation scheme E, FeCl₂ could be uniformly distributed on the surface of the CTW, which improved its utilization rate and greatly reduced the conventional dosage of activating agent (An et al. 2018). However, for impregnation scheme D, equivalent FeCl₂ was not enough, that was, CTW was not sufficiently impregnated with FeCl₂, and there were smooth areas in AC-DI. Furthermore, a small amount of FeCl₂ also accumulated due to uneven distribution, which caused overactivation on CTW, leading to obvious cracks in AC-DI (Wang and Wang 2019). The AC-AE showed better pore structure than AC-DI, which further proved that AE dissolution improved the activation efficiency of FeCl₂.

Crystalline phase composition

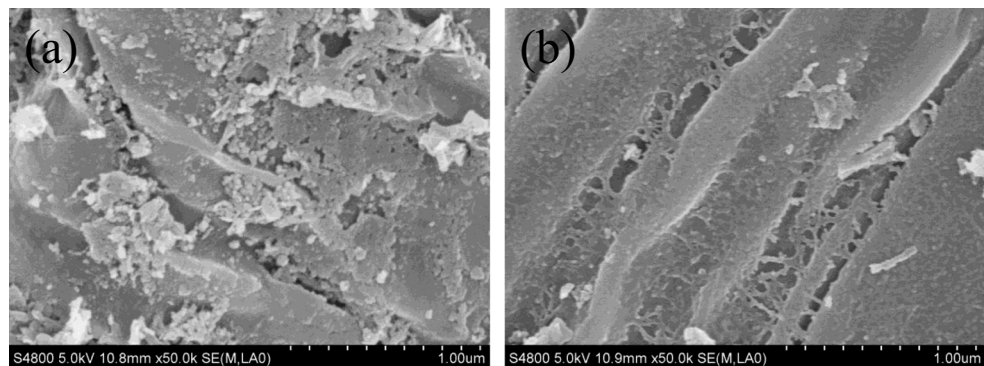
The XRD patterns of the ACs are presented in Fig. 6. As seen in AC-AE and AC-DI, the two broad peaks at 23.741° and 42.128°, features of the disordered graphite plane (002) and graphite plane (100), showed that the cellulose structure and organic matter in CTW were destroyed and transformed during pyrolysis (Yang et al. 2019). Compared with the AC-DI, the intensity of the 002 and 100 peaks of AC-AE gradually increased. The former peak was due to the amorphous structure of carbon structures in ACs, while such amorphism was conducive to the formation of microporous channels (Wang et al. 2014). The calculated interplanar distance of 002 was

$d_{\text{AC-DI}} (0.311) < 0.335 < d_{\text{AC-AE}} (0.440)$, which indicated that AC-AE showed a high degree of disorder. In impregnation scheme E, CTW was uniformly activated, which made the orientation of disordered structure more random in the carbonization process of forming a six-membered ring carbon network (Lee et al. 2014). The appearance of the later peak (100) was caused by graphite microcrystalline; the smaller microcrystalline was more obvious in AC-AE, which was considered to support the graphite pore walls (Gao et al. 2013). In the microcrystal dimensions' parameters, $L_{\text{AC-AE}} (0.354) < L_{\text{AC-DI}} (0.678)$, it showed that AC-AE showed better crystallization. It has been reported that the presence of metal compounds could reduce the barrier of the solid-state transition from amorphous carbon to graphene because the amorphous carbon was absorbed by the metal crystal, and the graphene layer nucleated and grown in its surface (Gai et al. 2017). AE improved the activation efficiency of FeCl₂; thus, AC-AE observed more graphite carbon structure. Hence, impregnation scheme E could produce an AC with improved structural characteristics where the superior crystalline phase would be available to form a developed porous structure in ACs.

Surface functional groups

The FTIR spectra of ACs are presented in Fig. 7. At 3431 cm⁻¹, the O–H vibration strength of carboxyl, phenol, and absorbed water for the AC-AE was weakened, thereby illustrating that AE dissolving FeCl₂ efficiently destroyed the glycosidic bond and hydrogen bond in CTW to form monosaccharide or disaccharide and enhanced the dehydration of saccharides, and more O–H was removed (Wang et al. 2017; Xu et al. 2019). The higher O–H in AC-DI was due to the low activation effect of FeCl₂, which led to the ineffective decomposition and dehydration of CTW. The

Fig. 5 The SEM of AC-AE (a) and AC-DI (b)



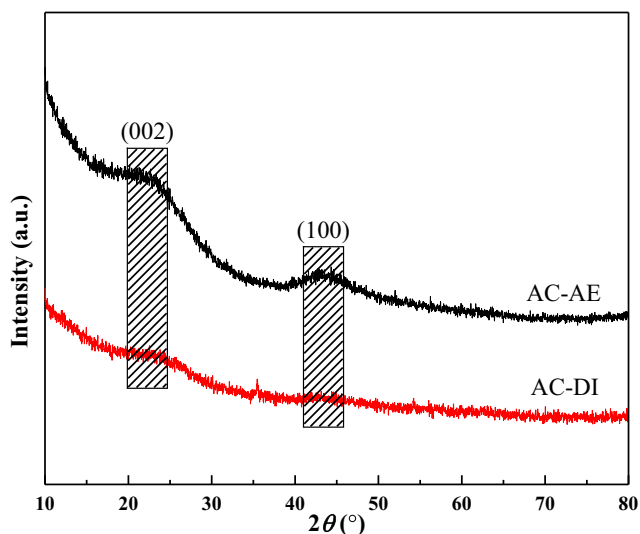


Fig. 6 XRD patterns of AC-AE and AC-DI

bands at approximately 2907 cm^{-1} correspond to the stretching vibration of $-\text{CH}_3$ and $-\text{CH}_2$, and the band at approximately 1620 cm^{-1} was attributed to aromatic $\text{C}=\text{C}$ stretching vibrations (Yang et al. 2019). It should be noted that the stretching vibration of $-\text{CH}_3$ and $-\text{CH}_2$ in AC-AE was weaker than that in AC-DI, while the aromatic $\text{C}=\text{C}$ was enhanced. This might be because AE provided FeCl_2 to play a critical role in CTW. In detail, the CTW underwent condensation and rearrangement reaction, and most of the functional groups on the surface of the carbon matrix were damaged. Finally, the residual solid was mainly the aromatic ring structure linked with methyl and methylene groups (Zhang et al. 2018). In impregnation scheme E, FeCl_2 promoted further polycondensation of the aforementioned aromatic ring structure, resulting in the disappearance of the bonding group and the formation of highly aromatic polymeric carbon

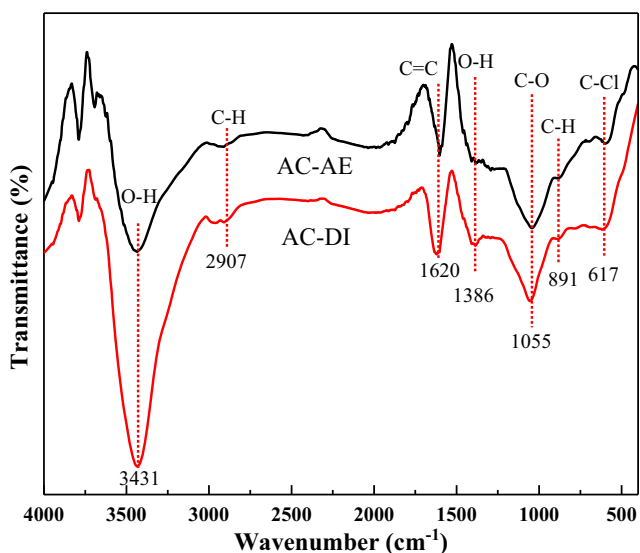


Fig. 7 FTIR spectra analysis of AC-AE and AC-DI

(Yang et al. 2019). Additionally, the bonds at 1386 cm^{-1} were characteristic of $\text{O}-\text{H}$ in phenolic hydroxyl, and its peak in AC-AE was weak because the phenolic hydroxyls could be dehydrated. Based on the analysis of intensity and species of surface functional groups on the ACs, it was inferred that the surface properties of ACs prepared by impregnation scheme E were superior.

Adsorption studies

Effect of pH

Figure S1 describes the effect of the initial pH on the adsorption of Cr(VI) . It could be found that the adsorption trends of both ACs were similar, and the adsorption capacity reduced with the increase of initial pH value. The pH value at 2–3, Cr(VI) anion mainly existed as HCr_2O_4^- that was the main form involved in the surface reduction and adsorption and exhibited excellent adsorbability on AC surface (Monser and Adhoum 2009). Thus, the maximum adsorption capacity was reached in this pH range. With the pH value increased, the main form of Cr(VI) changed to CrO_4^{2-} ; it might have competitive adsorption with OH^- on the AC surface, making the adsorption of Cr(VI) unremarkable (Mohan et al. 2005). Notably, the adsorption capacity of AC-AE was higher than AC-DI at whole pH values (2–7), because the former exhibited higher pH_{pzc} (AC-AE:5.6, AC-DI:1.9). As the initial pH exceeded pH_{pzc} , the surface electropositivity gradually changed to electronegativity, which weakened the electrostatic effect of ACs on anions (Huang et al. 2009). Importantly, impregnation scheme E contributed to better preparation of the AC-AE with superior pore structure and surface characteristics. In fact, the abundant microporous structure and a small number of acid functional groups were beneficial for increasing the contact area between the ACs and the Cr(VI) and providing more adsorption sites (Acosta et al. 2016).

Adsorption kinetics

As seen in Fig. S2, the Cr(VI) was rapidly adsorbed within the initial 30 min and then tended to be gentle. This was because the concentration gradient of Cr(VI) on ACs was large at the initial stage of adsorption. As Cr(VI) occupied all adsorption sites, it began to diffuse radially to the inner channel with high mass transfer resistance, resulting in slow adsorption until finally reaching adsorption equilibrium (Theydan and Ahmed 2012). The pseudo-first-order and pseudo-second-order models were applied to determine the adsorption properties of ACs toward Cr(VI) . The kinetic parameters are displayed in Table 5. According to the relative coefficient (R^2), the pseudo-second-order model was more suitable for describing the adsorption kinetic process, suggesting that chemisorption occurred during the adsorption process (Miao

Table 5 Adsorption kinetics model parameters of ACs

Samples	Pseudo-first-order			Pseudo-second-order		
	q_e (mg/g)	k_1 (min ⁻¹)	R^2	q_e (mg/g)	k_2 (g min/mg)	R^2
AC-AE	3.729	0.006	0.734	21.485	0.013	0.999
AC-DI	11.492	0.017	0.876	15.681	0.007	0.999

et al. 2016). It could be found that the calculated values (q_e) of AC-AE and AC-DI (21.485, 15.681 mg/g) estimated from the pseudo-second-order model displayed good agreement with the experimental values (21.401, 15.587 mg/g) of Cr(VI). Moreover, the calculated q_e values of AC-AE were higher than that of AC-DI; these results suggested that AE dissolution improved the pore structure and surface properties of AC-AE and provided additional active sites for Cr(VI) adsorption (Gao et al. 2013). Additionally, the high values of adsorption rates (k_2) were obtained for AC-AE, indicating faster adsorption kinetics for it. Based on that, it was confirmed that AC-AE prepared by AE dissolving FeCl₂ possessed superior pore structure and surface characteristics and displayed better adsorption capacity for Cr(VI).

Adsorption isotherms

In Fig. S3, the Langmuir and Freundlich models were used to explain the adsorption process in the adsorption isotherm study. The isotherm parameters are calculated and listed in Table 6. Based on the value of R^2 , the adsorption behavior of Cr(VI) onto ACs was fitted with the Langmuir model, revealing that the adsorption process was mainly controlled by the homogeneous monolayer adsorption (Islam et al. 2017a). From Table 6, the maximum adsorption amount of AC-AE (137.289 mg/g) for Cr(VI) was much higher than AC-DI (91.550 mg/g). This demonstrated that AC-AE with excellent surface properties were beneficial for removing Cr(VI). An important observation from the calculated values of R_L was that the adsorption of Cr(VI) onto AC-AE was more favorable than that of AC-DI due to the homogeneous surface of the former. Moreover, as the R_L was close to zero, the adsorption was almost irreversible (Feng et al. 2011). Overall, the AC-AE synthesized by impregnation scheme E, it composited with

high specific surface areas and microporous structure exhibited high adsorption capacities for Cr(VI) removal.

Table 7 provides a comparison of the maximum Cr(VI) adsorption capacities of different activated carbons reported in recent years. The maximum adsorption capacity for Cr(VI) of AC-AE was higher than other ACs derived from different precursors, suggesting that developing AC from CTW by FeCl₂ impregnation activation after AE dissolution was a promising method for removing Cr(VI).

Magnetization and reusability

Magnetization

The recyclability was an important property of MAC, which could be greatly improved in the presence of magnetism (Siddiqui et al. 2018). As seen in Fig. 8, it was found that nonlinear and reversible behavior with a weak magnetic hysteresis loop was observed. MAC exhibited a higher value of saturation magnetization (M_s) of 17.727 emu/g, remanence (M_r) of 0.527 emu/g, and 90.204 Oe of coercivity (H_c) that enabled MAC an easy separability by means of a magnet. The M_s value of MAC was higher than that of magnetic carbon previously reported (Siddiqui et al. 2018). Because impregnation scheme E provided more FeCl₂ to participate in the transformation and evolution of iron species and form more stable and homogeneous iron-carbon structures (Reguyal et al. 2017). Furthermore, the ratio of M_r/M_s was 0.03, indicating that MAC was superparamagnetic at room temperature and easy to magnetize and demagnetize (Ranjithkumar et al. 2014). Herein, MAC exhibited an excellent recovery and was easy to separate solid-liquid after adsorption, which demonstrated that FeCl₂ could endow ACs with higher magnetism.

Table 6 Adsorption isotherm model parameters of ACs

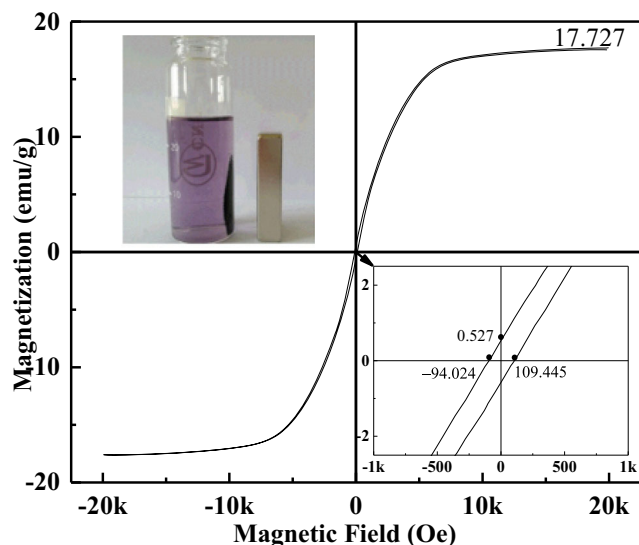
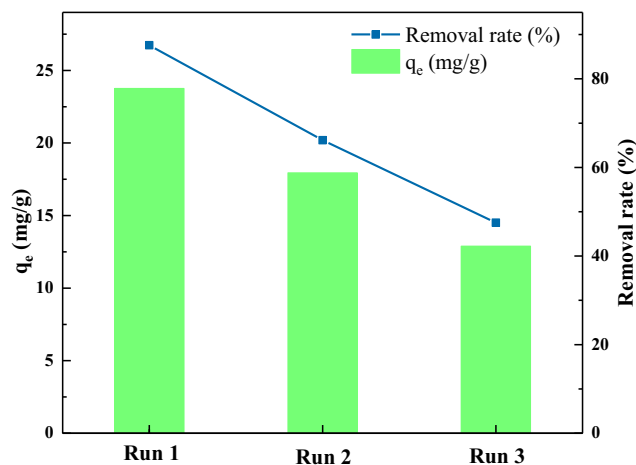
Samples	Langmuir				Freundlich		
	q_m (mg/g)	k_L (L/mg)	R_L	R^2	K_F ((mg/g) (mg/L) ^{-1/n})	n	R^2
AC-AE	137.289	0.012	0.625	0.948	10.710	2.674	0.898
AC-DI	91.550	0.010	0.167	0.938	7.659	5.532	0.844

Table 7 Comparison of the maximum Cr(VI) adsorption capacities (q_m) of different activated carbons

Activated carbons	q_m (mg/g)	References
Chestnut oak shells activated carbon	85.47	Niazi et al. (2018)
Nitric acid modified activated carbon	48.00	Valentin-Reyes et al. (2019)
Bamboo bark activated carbon	19.53	Zhang et al. (2015)
Corncob activated carbon	9.625	Li et al. (2018a)
Peanut hull activated carbon	77.5	Han et al. (2016)
Fox nutshell activated carbon	43.45	Kumar and Jena (2017)
AC-DI	91.55	This study
AC-AE	137.289	This study

Reusability

Reusability and stability are crucial for MAC used in pollutant adsorption. The prepared MAC was used for the adsorption/desorption experiments to evaluate its reusability. As illustrated in Fig. 9, MAC was stable and maintained normal adsorption efficiency in the first two rounds of the tests. In the 3rd run, the adsorption ability of MAC became insufficient, mainly due to MAC deactivation via the deposition of small molecular contaminants onto its surface and internal (Zhang et al. 2018). In run 3, the adsorption capacity could reach 59.574% of the initial adsorption capacity. Even after three times of recycling, MAC still maintained adsorption capacities of 13.524 mg/g for Cr(VI), which were still higher than that of some common absorbents (Celik et al. 2004). Therefore, MAC had a strong potential for adsorption applications, as it had facile magnetic separability and good recyclability.

**Fig. 8** Magnetization curves of the MAC**Fig. 9** Reusability of the MAC

Conclusion

In this work, ACs were prepared by one-step activation pyrolysis using CTW precursor and FeCl₂ impregnation activation after AE dissolution, respectively. The optimal conditions were obtained by orthogonal experiment as the mass ratio of 0.5:1, the activation temperature of 600 °C, and the activation time of 1 h. The prepared ACs under the optimal condition were compared with the control group (deionized water instead of AE). The results indicated that the dissolution of AE could reduce the aggregation and dosage of FeCl₂, and remarkably improved the activation efficiency, and the ACs exhibited superior physicochemical performances. Additionally, FeCl₂ enhanced the decomposition of volatile substances in CTW to produce gaseous products and then formed developed micropores that could also be attributed to the improvement of the graphite crystalline phase by FeCl₂, providing a carrier for pore diffusion path. The adsorption behavior toward Cr(VI) with the pseudo-second-order kinetic and the Langmuir isotherm indicated that the adsorption performance was favorable and efficient for the ACs. Furthermore, the iron oxides loaded on the carbon matrix with the evolution of the iron species were beneficial for improving the recyclability of magnetic ACs.

Funding information This work was financed by the National Natural Science Foundation of China (21707090) and the Chinese Postdoctoral Science Foundation (2017M611590).

References

- Acosta R, Fierro V, Martinez de Yuso A, Nabarlatz D, Celzard A (2016) Tetracycline adsorption onto activated carbons produced by KOH

- activation of tyre pyrolysis char. *Chemosphere* 149:168–176. <https://doi.org/10.1016/j.chemosphere.2016.01.093>
- An GH, Kim H, Ahn HJ (2018) Improved ionic diffusion through the mesoporous carbon skin on silicon nanoparticles embedded in carbon for ultrafast lithium storage. *ACS Appl Mater Interfaces* 10:6235–6244. <https://doi.org/10.1021/acsami.7b15950>
- Cagnon B, Py X, Guillot A, Stoeckli F, Chambat G (2009) Contributions of hemicellulose, cellulose and lignin to the mass and the porous properties of chars and steam activated carbons from various lignocellulosic precursors. *Bioresour Technol* 100:292–298. <https://doi.org/10.1016/j.biortech.2008.06.009>
- Celik A, Dost K, Sezer H (2004) An investigation of chromium(VI) ion removal from wastewaters by adsorption on residual lignin. *Fresenius Environ Bull* 13:124–127
- Devi P, Saroha AK (2014) Synthesis of the magnetic biochar composites for use as an adsorbent for the removal of pentachlorophenol from the effluent. *Bioresour Technol* 169:525–531. <https://doi.org/10.1016/j.biortech.2014.07.062>
- Dong H, Deng J, Xie Y, Zhang C, Jiang Z, Cheng Y, Hou K, Zeng G (2017) Stabilization of nanoscale zero-valent iron (nZVI) with modified biochar for Cr(VI) removal from aqueous solution. *J Hazard Mater* 332:79–86. <https://doi.org/10.1016/j.jhazmat.2017.03.002>
- Feng Y, Yang F, Wang Y, Ma L, Wu Y, Kerr PG, Yang L (2011) Basic dye adsorption onto an agro-based waste material-sesame hull (*Sesamum indicum* L.). *Bioresour Technol* 102:10280–10285. <https://doi.org/10.1016/j.biortech.2011.08.090>
- Feng L, Zhao L, Lee SH (2020) Dispersion behavior of HfC-based nanopowders in ethanol. *Int J Appl Ceram Technol* 17:1498–1504. <https://doi.org/10.1111/ijac.13409>
- Gai C, Zhang F, Lang QQ, Liu TT, Peng NN, Liu ZG (2017) Facile one-pot synthesis of iron nanoparticles immobilized into the porous hydrochar for catalytic decomposition of phenol. *Appl Catal B Environ* 204:566–576. <https://doi.org/10.1016/j.apcatb.2016.12.005>
- Gao Y, Yue Q, Gao B, Sun Y, Wang W, Li Q, Wang Y (2013) Comparisons of porous, surface chemistry and adsorption properties of carbon derived from *Enteromorpha prolifera* activated by $H_4P_2O_7$ and KOH. *Chem Eng J* 232:582–590. <https://doi.org/10.1016/j.cej.2013.08.011>
- Han YT, Cao X, Ouyang X, Sohi SP, Chen JW (2016) Adsorption kinetics of magnetic biochar derived from peanut hull on removal of Cr(VI) from aqueous solution: effects of production conditions and particle size. *Chemosphere* 145:336–341. <https://doi.org/10.1016/j.chemosphere.2015.11.050>
- Han S, Zang Y, Gao Y, Yue Q, Zhang P, Kong W, Jin B, Xu X, Gao B (2020) Co-monomer polymer anion exchange resin for removing Cr(VI) contaminants: adsorption kinetics, mechanism and performance. *Sci Total Environ* 709:136002. <https://doi.org/10.1016/j.scitotenv.2019.136002>
- He X, Li R, Qiu J, Xie K, Ling P, Yu M, Zhang X, Zheng M (2012) Synthesis of mesoporous carbons for supercapacitors from coal tar pitch by coupling microwave-assisted KOH activation with a MgO template. *Carbon* 50:4911–4921. <https://doi.org/10.1016/j.carbon.2012.06.020>
- Huang G, Shi JX, Langrish TAG (2009) Removal of Cr(VI) from aqueous solution using activated carbon modified with nitric acid. *Chem Eng J* 152:434–439. <https://doi.org/10.1016/j.cej.2009.05.003>
- Ilyas SU, Pendyala R, Marneni N (2014) Dispersion behaviour and agglomeration effects of zinc oxide nanoparticles in ethanol-water mixtures. *Mater Res Innov* 18:179–183. <https://doi.org/10.1179/1432891714Z.000000000953>
- Islam MA, Ahmed MJ, Khanday WA, Asif M, Hameed BH (2017a) Mesoporous activated carbon prepared from NaOH activation of rattan (*Lacosperma secundiflorum*) hydrochar for methylene blue removal. *Ecotoxicol Environ Saf* 138:279–285. <https://doi.org/10.1016/j.ecoenv.2017.01.010>
- Islam MA, Ahmed MJ, Khanday WA, Asif M, Hameed BH (2017b) Mesoporous activated coconut shell-derived hydrochar prepared via hydrothermal carbonization-NaOH activation for methylene blue adsorption. *J Environ Manag* 203:237–244. <https://doi.org/10.1016/j.jenvman.2017.07.029>
- Kumar A, Jena HM (2017) Adsorption of Cr(VI) from aqueous phase by high surface area activated carbon prepared by chemical activation with $ZnCl_2$. *Process Saf Environ Prot* 109:63–71. <https://doi.org/10.1016/j.psep.2017.03.032>
- Lam SS, Liew RK, Wong YM, Yek PNY, Ma NL, Lee CL, Chase HA (2017) Microwave-assisted pyrolysis with chemical activation, an innovative method to convert orange peel into activated carbon with improved properties as dye adsorbent. *J Clean Prod* 162:1376–1387. <https://doi.org/10.1016/j.jclepro.2017.06.131>
- Lee T, Zubir ZA, Jamil FM, Matsumoto A, Yeoh F-Y (2014) Combustion and pyrolysis of activated carbon fibre from oil palm empty fruit bunch fibre assisted through chemical activation with acid treatment. *J Anal Appl Pyrolysis* 110:408–418. <https://doi.org/10.1016/j.jaap.2014.10.010>
- Li HY, Gao P, Cui JG, Zhang F, Wang F, Cheng JC (2018a) Preparation and Cr(VI) removal performance of corncob activated carbon. *Environ Sci Pollut Res* 25:20743–20755. <https://doi.org/10.1007/s11356-018-2026-y>
- Li M, Suriel I, Vekaria J, Proske J, Orbe P, Armani M, Dave RN, Bilgili E (2018b) Impact of dispersants on dissolution of itraconazole from drug-loaded, surfactant-free, spray-dried nanocomposites. *Powder Technol* 339:281–295. <https://doi.org/10.1016/j.powtec.2018.08.014>
- Liang H, Sun R, Song B, Sun Q, Peng P, She D (2020) Preparation of nitrogen-doped porous carbon material by a hydrothermal-activation two-step method and its high-efficiency adsorption of Cr(VI). *J Hazard Mater* 387:121987. <https://doi.org/10.1016/j.jhazmat.2019.121987>
- Liew RK, Azwar E, Yek PNY, Lim XY, Cheng CK, Ng JH, Jusoh A, Lam WH, Ibrahim MD, Ma NL, Lam SS (2018) Microwave pyrolysis with KOH/NaOH mixture activation: a new approach to produce micro-mesoporous activated carbon for textile dye adsorption. *Bioresour Technol* 266:1–10. <https://doi.org/10.1016/j.biortech.2018.06.051>
- Manohara HM, Aruchamy K, Chakraborty S, Radha N, Nidhi MR, Ghosh D, Nataraj SK, Mondal D (2019) Sustainable water purification using an engineered solvothermal carbon based membrane derived from a eutectic system. *ACS Sustain Chem Eng* 7:10143–10153. <https://doi.org/10.1021/acssuschemeng.9b01983>
- Miao M-s, Wang Y-n, Kong Q, Shu L (2016) Adsorption kinetics and optimum conditions for Cr(VI) removal by activated carbon prepared from luffa sponge. *Desalin Water Treat* 57:7763–7772. <https://doi.org/10.1080/19443994.2015.1015453>
- Mohan D, Singh KP, Singh VK (2005) Removal of hexavalent chromium from aqueous solution using low-cost activated carbons derived from agricultural waste materials and activated carbon fabric cloth. *Ind Eng Chem Res* 44:1027–1042. <https://doi.org/10.1021/ie0400898>
- Monser L, Adhoum N (2009) Tartrazine modified activated carbon for the removal of Pb(II), Cd(II) and Cr(III). *J Hazard Mater* 161:263–269. <https://doi.org/10.1016/j.jhazmat.2008.03.120>
- Muniz G, Fierro V, Celzard A, Furdin G, Gonzalez-Sanchez G, Ballinas ML (2009) Synthesis, characterization and performance in arsenic removal of iron-doped activated carbons prepared by impregnation with Fe(III) and Fe(II). *J Hazard Mater* 165:893–902. <https://doi.org/10.1016/j.jhazmat.2008.10.074>
- Niazi L, Lashanizadegan A, Shariffifar H (2018) Chestnut oak shells activated carbon: preparation, characterization and application for Cr(VI) removal from dilute aqueous solutions. *J Clean Prod* 185:554–561. <https://doi.org/10.1016/j.jclepro.2018.03.026>

- Ohmukai Y, Hasegawa I, Fujisawa H, Okuma O, Mae K (2008) Production of an iron-loaded carbonaceous material through pyrolyzing biomass impregnated with FeCl₂. *Fuel* 87:2041–2049. <https://doi.org/10.1016/j.fuel.2007.12.013>
- Raiteri P, Laio A, Parrinello M (2004) Correlations among hydrogen bonds in liquid water. *Phys Rev Lett* 93:087801. <https://doi.org/10.1103/PhysRevLett.93.087801>
- Ranjithkumar V, Sangeetha S, Vairam S (2014) Synthesis of magnetic activated carbon/alpha-Fe₂O₃ nanocomposite and its application in the removal of acid yellow 17 dye from water. *J Hazard Mater* 273:127–135. <https://doi.org/10.1016/j.jhazmat.2014.03.034>
- Reguyal F, Sarmah AK, Gao W (2017) Synthesis of magnetic biochar from pine sawdust via oxidative hydrolysis of FeCl₂ for the removal of sulfamethoxazole from aqueous solution. *J Hazard Mater* 321:868–878. <https://doi.org/10.1016/j.jhazmat.2016.10.006>
- Rufford TE, Hulicova-Jurcakova D, Zhu Z, Lu GQ (2010) A comparative study of chemical treatment by FeCl₃, MgCl₂, and ZnCl₂ on microstructure, surface chemistry, and double-layer capacitance of carbons from waste biomass. *J Mater Res* 25:1451–1459. <https://doi.org/10.1557/JMR.2010.0186>
- Shi YW, Liu GZ, Wang L, Zhang HW (2019) Activated carbons derived from hydrothermal impregnation of sucrose with phosphoric acid: remarkable adsorbents for sulfamethoxazole removal. *RSC Adv* 9:17841–17851. <https://doi.org/10.1039/c9ra02610j>
- Siddiqui MTH, Nizamuddin S, Baloch HA, Mubarak NM, Dumbre DK, Inamuddin, Asiri AM, Bhutto AW, Srinivasan M, Griffin GJ (2018) Synthesis of magnetic carbon nanocomposites by hydrothermal carbonization and pyrolysis. *Environ Chem Lett* 16:821–844. <https://doi.org/10.1007/s10311-018-0724-9>
- Theydan SK, Ahmed MJ (2012) Adsorption of methylene blue onto biomass-based activated carbon by FeCl₃ activation: equilibrium, kinetics, and thermodynamic studies. *J Anal Appl Pyrolysis* 97:116–122. <https://doi.org/10.1016/j.jaap.2012.05.008>
- Tian D, Xu Z, Zhang D, Chen W, Cai J, Deng H, Sun Z, Zhou Y (2019) Micro-mesoporous carbon from cotton waste activated by FeCl₃/ZnCl₂: preparation, optimization, characterization and adsorption of methylene blue and eriochrome black T. *J Solid State Chem* 269:580–587. <https://doi.org/10.1016/j.jssc.2018.10.035>
- Tseng HH, Su JG, Liang C (2011) Synthesis of granular activated carbon/zero valent iron composites for simultaneous adsorption/dechlorination of trichloroethylene. *J Hazard Mater* 192:500–506. <https://doi.org/10.1016/j.jhazmat.2011.05.047>
- Valentin-Reyes J, Garcia-Reyes RB, Garcia-Gonzalez A, Soto-Regalado E, Cerino-Cordova F (2019) Adsorption mechanisms of hexavalent chromium from aqueous solutions on modified activated carbons. *J Environ Manag* 236:815–822. <https://doi.org/10.1016/j.jenvman.2019.02.014>
- Wang J, Wang S (2019) Preparation, modification and environmental application of biochar: a review. *J Clean Prod* 227:1002–1022. <https://doi.org/10.1016/j.jclepro.2019.04.282>
- Wang S, Liu Q, Liao Y, Luo Z, Cen K (2007) A study on the mechanism research on cellulose pyrolysis under catalysis of metallic salts. *Korean J Chem Eng* 24:336–340. <https://doi.org/10.1007/s11814-007-5060-x>
- Wang L, Zhang Z, Qu Y, Guo Y, Wang Z, Wang X (2014) A novel route for preparation of high-performance porous carbons from hydrochars by KOH activation. *Colloids Surf A Physicochem Eng Asp* 447:183–187. <https://doi.org/10.1016/j.colsurfa.2014.01.013>
- Wang J, Liu T-L, Huang Q-X, Ma Z-Y, Chi Y, Yan J-H (2017) Production and characterization of high quality activated carbon from oily sludge. *Fuel Process Technol* 162:13–19. <https://doi.org/10.1016/j.fuproc.2017.03.017>
- Wu L, Liao L, Lv G, Qin F, He Y, Wang X (2013) Micro-electrolysis of Cr(VI) in the nanoscale zero-valent iron loaded activated carbon. *J Hazard Mater* 254:277–283. <https://doi.org/10.1016/j.jhazmat.2013.03.009>
- Xia XF, Zhang K, Xiao HR, Xiao SW, Song ZY, Yang ZY (2019) Effects of additives and hydrothermal pretreatment on the pelleting process of rice straw: energy consumption and pellets quality. *Ind Crop Prod* 133:178–184. <https://doi.org/10.1016/j.indcrop.2019.03.007>
- Xu Z, Zhang T, Yuan Z, Zhang D, Sun Z, Huang YX, Chen W, Tian D, Deng H, Zhou Y (2018) Fabrication of cotton textile waste-based magnetic activated carbon using FeCl₃ activation by the Box-Behnken design: optimization and characteristics. *RSC Adv* 8:38081–38090. <https://doi.org/10.1039/c8ra06253f>
- Xu Z, Zhou Y, Sun Z, Zhang D, Huang Y, Gu S, Chen W (2019) Understanding reactions and pore-forming mechanisms between waste cotton woven and FeCl₃ during the synthesis of magnetic activated carbon. *Chemosphere* 241:125120. <https://doi.org/10.1016/j.chemosphere.2019.125120>
- Yang B, Liu Y, Liang Q, Chen M, Ma L, Li L, Liu Q, Tu W, Lan D, Chen Y (2019) Evaluation of activated carbon synthesized by one-stage and two-stage co-pyrolysis from sludge and coconut shell. *Ecotoxicol Environ Saf* 170:722–731. <https://doi.org/10.1016/j.ecoenv.2018.11.130>
- Zhang YJ, Ou JL, Duan ZK, Xing ZJ, Wang Y (2015) Adsorption of Cr(VI) on bamboo bark-based activated carbon in the absence and presence of humic acid. *Colloid Surface A Physicochem Eng Asp* 481:108–116. <https://doi.org/10.1016/j.colsurfa.2015.04.050>
- Zhang H, Xue G, Chen H, Li X (2018) Magnetic biochar catalyst derived from biological sludge and ferric sludge using hydrothermal carbonization: preparation, characterization and its circulation in Fenton process for dyeing wastewater treatment. *Chemosphere* 191:64–71. <https://doi.org/10.1016/j.chemosphere.2017.10.026>
- Zhang WF, Zhang PX, Liu F, Liu WZ, Zhang J, Lin Z (2019) Simultaneous oxidation of Cr(III) and extraction of Cr(VI) from chromite ore processing residue by silicate-assisted hydrothermal treatment. *Chem Eng J* 371:565–574. <https://doi.org/10.1016/j.cej.2019.04.082>

Publisher's note Springer Nature remains neutral with regard to jurisdictional claims in published maps and institutional affiliations.